Energy band gap, intrinsic carrier concentration, and Fermi level of CdTe bulk crystal between 304 and 1067 K

Article *in* Journal of Applied Physics · April 2008

DOI: 10.1063/1.2899087

CITATIONS
16

READS
2,340

1 author:

Ching-Hua Su
NASA, Marshall Space Flight Center
226 PUBLICATIONS **1,491** CITATIONS

SEE PROFILE

Energy band gap, intrinsic carrier concentration, and Fermi level of CdTe bulk crystal between 304 and 1067 K

Ching-Hua Su[a)]
EM30 Materials and Processing Laboratory, Engineering Directorate NASA/Marshall Space Flight Center, Huntsville, Alabama 35812, USA

(Received 20 June 2007; accepted 21 January 2008; published online 23 April 2008)

Optical transmission measurements were performed on CdTe bulk single crystals. It was found that when sliced and polished CdTe wafers were used, a white film started to develop on the sample surface and the wafer became opaque when it was heated above 530 K. Therefore, a bulk crystal of CdTe was first grown in the window area by physical vapor transport. The optical transmission was then measured between 304 and 1067 K and from which the energy band gap was derived. The band gaps of CdTe can fit well as a function of temperature by the Varshni expression. Using the band gap data, the high temperature electron-hole equilibrium was numerically calculated by assuming Kane's conduction band structure and a light-hole and a heavy-hole parabolic valence bands. The calculated intrinsic carrier concentrations agree well with the experimental data previously reported. The calculated intrinsic Fermi levels between 200 and 1200 K were also presented. [DOI: 10.1063/1.2899087]

I. INTRODUCTION

Due to the advantages of high resistivity and large band gap, CdTe as well as CdZnTe x-ray and gamma ray detectors can be operated at room temperature with excellent performance (see review articles[1,2]). However, the electro-optic properties of CdTe vary tremendously among crystals and are strongly influenced by the physics and chemistry of the materials during its growth process at elevated temperatures. For example, the intrinsic carrier concentration n_i and Fermi level at growth conditions can influence the doping efficiency as well as the degree of self-compensation from dopants and native point defects. Therefore, numerous studies on the defect chemistry and phase equilibria of CdTe at elevated temperatures have been reported.[3–11] For most of these analyses, the high temperature equilibrium between electron n and hole p was adopted by either (1) using an expression for the intrinsic carrier concentration[10,11] in the form typical for a nondegenerate semiconductor with parabolic conduction and valence bands, $n_i/T^{3/2}=K^0\exp(-H/kT)$ or (2) using a quasichemical reaction constant,[3–9] such as $np=K=K^0\exp(-H/kT)$, where K^0 and H are the adjustable parameters. In the first case, an energy band structure for CdTe was used to derive the intrinsic carrier concentrations by assuming the energy band gap extrapolating from the existing data at low temperature (below 300 K). In the quasichemical analyses, the best-fit value of H, sometimes erroneously interpreted as the energy band gap, varies from 1.5 (Refs. 8 and 9) to 1.73 (Ref. 3) and 1.92 eV.[4]

In this study, we determined the energy band gap of CdTe between 304 and 1067 K by optical transmission measurements. The results were expressed in terms of Varshni equation. With the energy band gap data, the high temperature electron-hole equilibrium was numerically calculated, without any assumption or adjustable parameters, by using Kane's conduction band structure and a light-hole and a heavy-hole parabolic valence bands. The calculated results on the intrinsic carrier concentrations as well as the intrinsic Fermi levels for CdTe between 200 and 1200 K are reported.

II. EXPERIMENT

A. Sample preparation

The optical cell, consisting of a window well and a side arm, was made of fused silica quartz. The window for the first optical cell, BG-1, with an interior well dimension of $15\times7.5\times1.7$ mm^3, was made by sandwiching a 1.7 mm thick cell edge between two 5 mm thick optical quartz windows. The window well was attached to an 18 mm outside diameter (o.d.) $\times$ 16 mm inside diameter (i.d.) fused silica tubing for the purpose of connecting to vacuum pump and sealoff. A wafer of CdTe, with dimension of $15\times7.5\times1.55$ mm^3, was sliced from a 20 mm diameter, twin-free, single crystal (111) CdTe rod provided by Keystone Crystal, Corp. The wafer was chemomechanical polished by 4% Br in ethylene glycol and then rinsed by de-ionized water. The empty cell was cleaned and baked at 1450 K under vacuum for 16 h. After the sample was loaded, the cell was sealed under a vacuum of 4×10^{-4} Torr. However, as the temperature increased above 530 K during the optical measurements, the overall optical transmission of the sample started to decrease and eventually, the sample became opaque. A white film was observed on the surfaces of the CdTe wafer after the cell was cooled down. Another optical cell, similar to BG-1 except a $10\times7.5\times1.04$ mm^3 (111) orientation CdTe single crystal provided by II-VI, Inc., was used. The sample also became opaque when the temperature was raised above 800 K. Therefore, a sample cell, BG-4, as shown in Fig. 1, was made by growing the CdTe wafer in the window well region using the physical vapor transport (PVT) technique.[12,13] For the CdTe starting material of the PVT

[a)]Electronic mail: ching.h.su@nasa.gov.

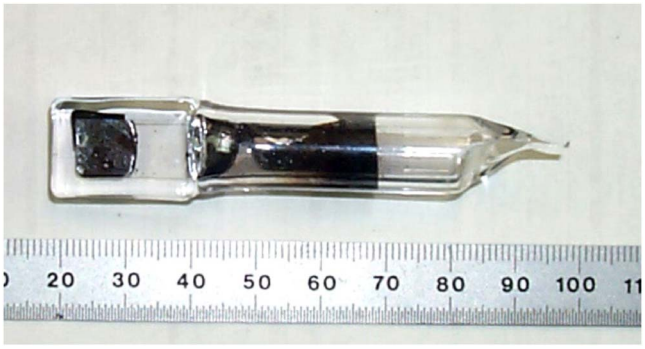

FIG. 1. (Color online) A picture of the CdTe optical cell BG-4 used in the optical measurements. The crystal in the window section (left side) was grown by physical vapor transport (PVT) from source material loaded in the side arm (right side).

process, the homogenization ampoule was made from fused silica tubing and was cleaned and outgassed at 1320 K under vacuum for over 16 h. The starting elements were quadruple zone refined (QZR), six-nine grade Cd rods and QZR, six-nine grade Te bars from Johnson Matthey, Inc. The batch (labeled as 7 in Ref. 14), consisting of 71.1613 g of Cd and 80.7791 g of Te, was loaded into the ampoule and sealed under vacuum. The sealed ampoule was then heated inside a furnace with an isothermal heat-pipe liner from room temperature to 1200 K in 4 h and maintained at 1200 K for 16 h before cool down. After the homogenization process, the ampoule was opened and the reacted spongelike CdTe was crushed and ground by mortar and pedestal into particles of diameter less than 0.5 mm. The optical cell window, with an interior well dimension of $17\times10\times1.5$ mm^3 was attached to a 12 mm o.d. $\times$ 8 mm i.d. fused silica tubing. After the cell was cleaned and baked out under vacuum, 5.84 g of CdTe from the batch was loaded, heat treated by annealing under 350 Torr of H_2 over pressure at 1143 K for 30 min, baking at 1143 K for 8 min under dynamic vacuum, and sealed under a vacuum of 4×10^{-4} Torr. The heat treatment procedure[14] would adjust the stoichiometry of the sample to near congruent sublimation condition, i.e., $P_{Cd}/P_{Te_2}=2.0$, to enhance the vapor transport rate. The growth by PVT was performed in a three-zone furnace[12] with the source at 1161 K, a thermal hump of 1167 K, and a cold zone of 1023 K. The furnace translation rate was 4 mm/day. After the growth, the cell was opened and sealed under vacuum to shorten its length from 18 to about 7 cm, as shown in Fig. 1.

B. Optical transmission measurements

The optical measurements, consisting of the assembly of a spectrophotometer and a T-shaped furnace in the arrangement of reverse optics, have been applied for the partial pressure measurements of the Zn–Se, HgI_2, Ga–Te, and Cd–Zn–Te systems and previously presented in detail.[15–19] The instrument has also been used to measure the optical transmission of a GaN single crystal between 293 and 1237 K to determine its band gap as a function of temperature.[20] The near-IR/visible/UV spectrophotometer (OLIS Inc., model 14H), shown in gray shade in Fig. 2, consists of a lamp

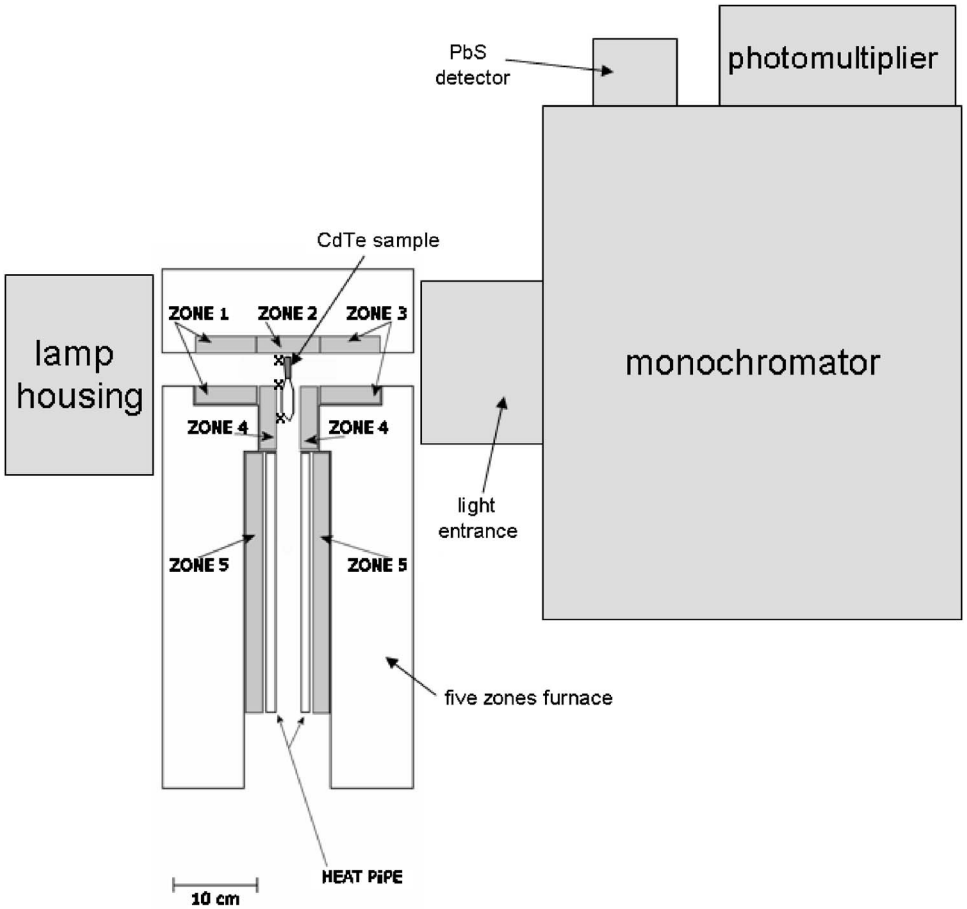

FIG. 2. The instrument for the transmission measurements. A halogen xenon lamp was positioned inside the lamp housing as the light source. Two mirrors inside the lamp housing reflect and focus the light into a sample beam, which passes through the sample cell in the furnace, and a reference beam which passes under the furnace. The monochromator and the photomultiplier/PbS detector act as the analyzer and detector, respectively. The sample cell was placed inside a five-zone T-shaped furnace. Three thermocouples, with their positions marked by x, were attached to the cell.

housing and a monochromator attached to a light entrance, an IR detector, and a photomultiplier. A halogen xenon lamp was positioned inside the lamp housing as the light source and the monochromator and a photomultiplier/PbS detector as the analyzer and detector. The sample cell was placed inside a five-zone T-shaped furnace with the window section at the top of the *T*, which consisted of three cylindrical heating zones with a total length of 30.5 cm. The bottom of the *T*, where the side arm of the cell is located, consisted of two cylindrical zones and was 47 cm long. Three thermocouples were attached to the cell, two next to the sample, and the other at the sealoff location. The temperatures of the five heating zones were independently controlled. During measurements, uniform temperature profiles were maintained inside the top of the *T* cavity. The whole window area of the cell was masked outside by a 3 mm thick ceramic fiber paper (FiberFrax 880) except for a 6 mm diameter hole where the sample was located. Two mirrors inside the lamp housing reflect and focus the light into a sample beam, which passes through the sample cell in the furnace, and a reference beam which passes under the furnace. The optical transmission spectra were measured between wavelengths of 820 and 1650 nm by the spectrophotometer. A series of transmission spectra was obtained between sample temperatures of 304 and 1067 K by taking the ratio of the intensity of the sample beam to that of the reference beam. The spectra were taken as the sample temperature increased with 15–20 min equilibration time at each set point. During the measurements at elevated temperature, the temperature profile along the optical cell was maintained with the sample end always at about 1–3 °C lower than the sealoff end to prevent sublimation from the sample. Since the CdTe sample was close to congruent sublimation, the heating of the sample during the measurements should not significantly change the sample composition. Also, the small free volume of the cell, about 0.65 cm^3, would only contain about 1 μg of Cd and 1.9 μg of Te in the vapor phase at the highest temperature of 1067 K, assuming that the sample is congruent subliming at 1067 K with partial pressures of Cd and Te_2 of about 2×10^{-3} and 1×10^{-3} atm, respectively.[21] A similar empty optical cell with the same fiber paper mask was positioned at the same location inside the furnace and the transmission spectrum was taken at 293 K as the base line. The absolute transmission spectra were determined from the ratio of the measured ones (with the sample) to the base line. The instrument band passes were 4.1, 2.9, 3.0, and 3.6 nm at wavelengths of 820, 1150, 1300, and 1650 nm, respectively.

III. RESULTS, ANALYSES, AND DISCUSSION

A. Optical transmission spectra

The absolute transmission spectra measured on the optical cell BG-4 are given in Fig. 3. The transmission-edge wavelength starts from about 850 nm for the spectrum of the lowest temperature, increasing as the sample temperature increases, to above 1200 nm for the spectrum at 1067 K. The origin of the subtle features at 960, 1260, and 1380 nm of the spectra is not clear. They might be related to the intrinsic properties of the optical windows, as suggested by the similar features exhibited by the base line, shown as dotted line in Fig. 3, taken on the empty cell. However, these features did not affect the band gap determination from the absorption edge except maybe only at the highest temperature curve by the feature at 1260 nm. The shapes of the transmission edges are similar for the runs from room temperature to 700 K. However, as the sample temperatures get above 800 K, as shown in Fig. 3, the slopes of the transmission edge became increasingly shallower and the total transmission became lower. Several spectra were taken at sample temperatures above 1067 K, not shown in Fig. 3, but the slope of the transmission edge was too shallow for a reliable determination of the energy band gap, as described in the next section. The total transmission at the high wavelength region also decreased as the sample temperature increased. After the measurements at elevated temperatures, the optical cell was taken out of the furnace and the sample surface was slightly duller than before the measurements. Under the optical microscope, the surface showed slight roughening. However, the surface changes should be minimal as the sample was grown at 1161 K in a similar thermal environment. In his thesis on the study of optical properties of silicon thin films and diamond layers, Remes[22] showed that the error of the absorption coefficient is proportional to the ratio of surface roughness to film thickness. Because our sample thickness, 1.5 mm, is much larger than his film thickness, in the order of 1 μm, the error caused by the slight roughness of our sample should be negligible. It was conceivable that the sample surface reflectivity changed either (1) as the surface characteristics evolved through heating process, which resulted in the changes in the optical transmission or (2) the intrinsic property of reflectivity is a function of temperature. However, as described in the next section, the absolute values of the transmission are not essential to the evaluation of the band gap, which was determined from the changes in the shapes of the absorption edges.

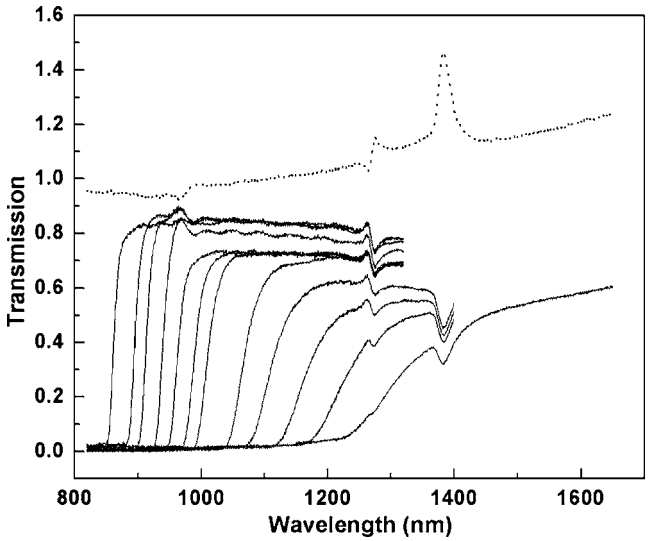

FIG. 3. The optical transmission spectra (solid curves) measured, from left to right, as the sample temperature increased. The dotted curve on the top was the single beam base line (arbitrary unit) measured on an empty cell under similar conditions at room temperature.

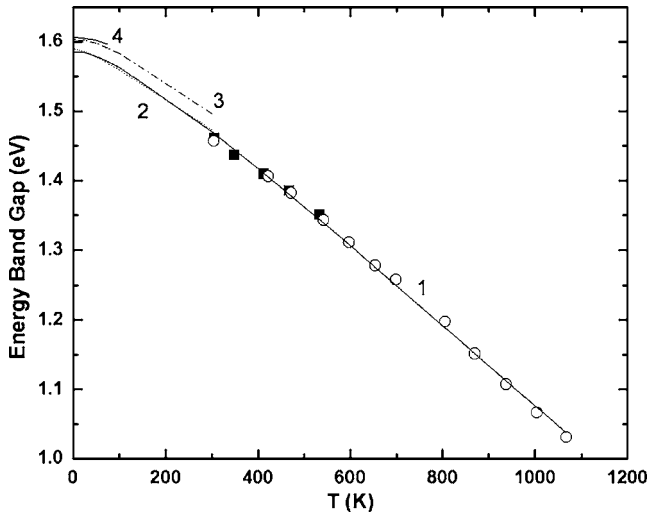

FIG. 4. The energy band gap of CdTe as a function of temperature. Solid squares are data from the cell BG-1 and open circles are from BG-4. Solid curve 1 is the energy band gap given by the best-fit Varshni expression [Eq. (3)]. The experimental data at low temperature are shown as the dotted curve 2 (Ref. 34), the dashed curve 3 (Ref. 35), and the short solid curve 4 (Ref. 36).

B. Energy band gap

The following equation was adopted to convert the measured transmission spectra to absorption spectra:

$$\mathrm{Tr} = (1-R)^2 \exp(-\alpha d)/[1-R^2 \exp(-2\alpha d)], \tag{1}$$

where Tr is the measured transmission, R is the reflectivity, α is the absorption coefficient, and d is the sample thickness. The optical properties of CdTe have been measured at room temperature by Adachi *et al.*[23] Since the reflectivity data in the range of 1–1.5 eV vary between 0.2 and 0.25, a value of 0.20 was used. The corresponding absorption spectrum was solved, using Eq. (1), from the reflectivity, the measured transmission spectrum, and sample thickness. The energy gap for each spectrum was determined from the derivative of the absorption coefficient with respect to energy E. The value of $d\alpha/dE$ started from zero in the low energy range, went through a maximum, and then rapidly dropped to a plateau of zero again. The band gap corresponds to the energy where the derivative decreases and just reaches the plateau.[20,24] The uncertainty in the determination of this energy is estimated to be ± 0.003 eV. This change of $d\alpha/dE$ as a function of energy E is essentially related to the Urbach absorption edge in that the Urbach edge corresponds to the ascending section of the $d\alpha/dE$ versus E curve. The energy width of this ascending section is related to the characteristic energy of the Urbach edge, which, in Einstein model, is a measure of the structural disorder. From the slopes of our data, this characteristic energy, or structural disorder, increases as the sample temperature increases. A similar trend was observed on the semi-insulating GaAs and InP crystals.[25]

The determined band gaps are plotted as symbols as a function of temperature in Fig. 4. The close agreement between the results from the two optical cells BG-1 and BG-4 shows the reproducibility in the band gap determined by our technique. Varshni[26] proposed that the major contribution to the temperature shift in the relative position of the conduction and valence bands is due to a temperature-dependent electron lattice interaction. This leads to a temperature dependence of band gap, E_g, in the form $E_g \propto T$ when $T \gg \theta$ and $E_g \propto T^2$ when $T \ll \theta$, where θ is the Debye temperature. Therefore, the following expression was proposed:

$$E_g = E_g(0) - \alpha T^2/(T+\beta), \tag{2}$$

where $E_g(0)$ is the band gap value at 0 K, α is a proportionality constant, and β is approximated to be the Debye temperature. Since our data lie in the medium to high temperature range, it would not be meaningful to determine the best-fit parameters by independently varying three parameters. The Debye temperature for CdTe has been reported as 158,[27,28] 161,[29] and 162.7 K.[30] Therefore, a value of 160 K was used and the experimental E_g data were plotted against $T^2/(T+160)$. A best linear fit was obtained to be

$$E_g(\mathrm{eV}) = 1.5860 - 5.9117 \times 10^{-4} T^2/(T+160), \tag{3}$$

with a standard deviation $\sqrt{\Sigma_{i=1}^{N}[E_{g,i}(\mathrm{obs}) - E_{g,i}(\mathrm{calc})]^2/(N-1)} = 0.006\,66$ eV. The calculated E_g from Eq. (3) is also plotted in Fig. 4 as solid curve 1. Our data cover most of the linear part of the Varshni equation which nonlinearly extrapolated toward the low temperature range. There were several experiments that reported the optical measurements of band gap for CdTe. These include those measurements on various CdTe thin films[31–33] and on bulk crystals.[34–36] As shown by Mathew,[31] that the measured band gap of CdTe strongly depends on the film thickness, from 1.526 eV for 0.2 μm thick film to 1.490 eV for 1.5 μm thick, we will only compare our results with the data on bulk crystals of CdTe, as given in Fig. 4. The dotted line (curve 2), which agrees well with our low temperature extrapolation, was determined from absorption edge measurements,[34] whereas the dashed line (curve 3) was determined from the measurements of photocurrent peak energies.[35] The low temperature data from Ref. 36, less than 80 K, shown as curve 4, were determined by a method similar to ours except that the band gap energy was picked at the maximum of the $d\alpha/dE$ versus E curve.

C. Theoretical calculation of intrinsic Fermi level and carrier concentration

Applying the band gap energy given by Eq. (3), the intrinsic Fermi level and carrier concentration are calculated using a procedure similar to the one given in Ref. 10. The heavy-hole valence band is taken to be parabolic with a hole density-of-state effective mass ratio of 0.66,[37] independent of temperature. The Ehrenberg approximation[38] for the Fermi–Dirac distribution was used for the heavy-hole valence band as an easy way of extending the validity of the calculations. The conduction and the light-hole valence bands are taken from the results of Kane's $k.p$ method.[39] Rather than using approximations for the secular energy[40–42] as done earlier, the wave number derivative of the band energy required to calculate the density of states was obtained using the exact cubic equation for the secular energy. Beside the band gap by Eq. (3) and the value of 0.66 for the heavy-hole effective mass, other parameters used for the calculation are 8.95

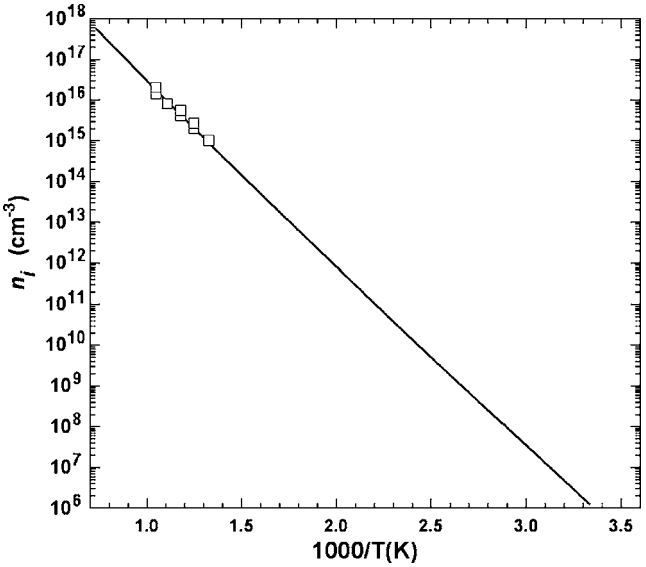

FIG. 5. The calculated intrinsic carrier concentrations are plotted against $1000/T$ (K). The squares are data reported by Smith (Ref. 45).

$\times 10^{-8}$ eV cm (Ref. 42) for the momentum matrix element and 0.81 eV (Refs. 43 and 44) for the spin-orbit splitting energy. A numerical calculation was performed by varying the Fermi level until the calculated sum of the heavy-hole concentration (by Ehrenberg approximation) and light-hole concentration (by numerically integrating the Fermi Dirac distribution through the density of states of the light-hole band) equals the calculated electron concentration (by numerically integrating through the density of states of the conduction band). The calculated intrinsic carrier concentration between 200 and 1200 K is plotted in Fig. 5 as a function of $1000/T$. The experimental data were performed by the Hall measurements at the elevated temperatures[45] and agree well with the calculated values. The calculated intrinsic carrier concentration can be fitted well by the expression for a nondegenerated semiconductor with parabolic bands as

$$\log_{10} n_i(\mathrm{cm}^{-3})T^{-3/2} = -4098.5/T + 16.064. \quad (4)$$

The corresponding intrinsic Fermi levels E_f^i/kT (k: Boltzmann constant) together with the band gap energy E_g/kT are shown in Fig. 6 as a function of T between 200 and 1200 K. The Fermi level changes from about $43kT$ below the conduction band at 200 K to $2.85kT$ below at 1200 K. Using the intrinsic Fermi level given here, the Fermi level for a nondegenerate, extrinsic (i.e., $n \neq p$)semiconductor at elevated temperatures can be derived by calculating the shift of Fermi level[10] given by the expression

$$E_f - E_f^i = -kT \sinh^{-1}[(p-n)/2n_i]. \quad (5)$$

In deriving Eq. (5), the relationship $np = n_i^2$ was used, which implies parabolic conduction and valence bands and the nondegenerate distributions. The full calculation using Kane's model described above has proven this assumption to be correct with sufficient accuracy.

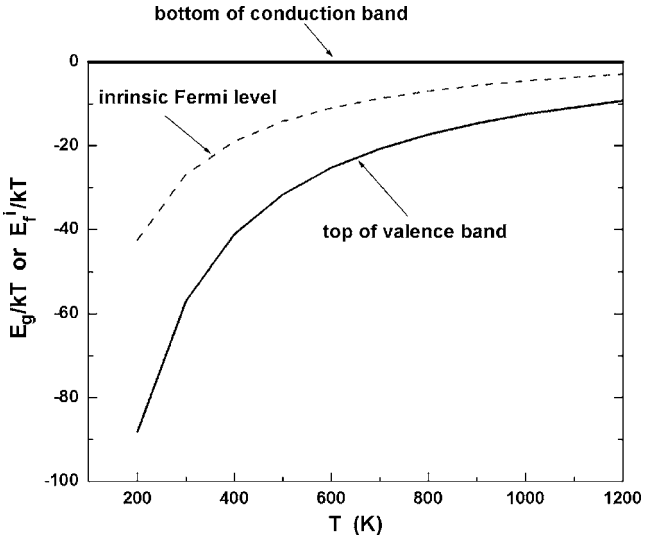

FIG. 6. The calculated intrinsic Fermi levels E_f^i/kT together with the band gap energy E_g/kT are shown as a function of T between 200 and 1200 K.

ACKNOWLEDGMENTS

The author would like to thank the contribution of Professor Brebrick of Marquette University for reviewing this manuscript and performing the intrinsic carrier concentration calculation with the inclusion of the light-hole valence band. The author would also like to acknowledge the supports of the Advanced Capabilities Division, Exploration Systems Mission Directorate, NASA Headquarter.

[1] P. Rudolph, Prog. Cryst. Growth Charact. Mater. **29**, 275 (1994).
[2] T. E. Schlesinger, J. E. Toney, H. Yoon, E. Y. Lee, B. A. Brunett, L. Franks, and R. B. James, Mater. Sci. Eng., R. **32**, 103 (2001).
[3] D. de Nobel, Philips Res. Rep. **14**, 361 (1959).
[4] S. S. Chern, H. R. Vydyanath, and F. A. Kroger, J. Solid State Chem. **14**, 33 (1975).
[5] S. S. Chern and F. A. Kroger, J. Solid State Chem. **14**, 44 (1975).
[6] F. A. Selim and F. A. Kroger, J. Electrochem. Soc. **124**, 401 (1977).
[7] Y. Marfaing, Phys. Rev. A **12**, 211 (1977).
[8] K. Zanio, *Cadmium Telluride, Semiconductors and Semimetals* (Academic, New York, 1978) p. 235.
[9] P. Fochuk, O. Korovyanko, and O. Panchuk, J. Cryst. Growth **197**, 603 (1999).
[10] C.-H. Su, P.-K. Liao, and R. F. Brebrick, J. Electron. Mater. **12**, 771 (1983).
[11] R. F. Brebrick and R. Fang, J. Phys. Chem. Solids **57**, 451 (1996).
[12] C.-H. Su, Proc. SPIE **3123**, 7 (1997).
[13] K. Chattopadhyay, S. Feth, H. Chen, A. Burger, and C.-H. Su, J. Cryst. Growth **191**, 377 (1998).
[14] C.-H. Su, Y.-G. Sha, S. L. Lehoczky, H.-C. Liu, R. Fang, and R. F. Brebrick, J. Cryst. Growth **183**, 519 (1998).
[15] C.-H. Su, W. Palosz, S. Feth, and S. L. Lehoczky, J. Cryst. Growth **192**, 386 (1998).
[16] C.-H. Su, S. Feth, and S. L. Lehoczky, J. Cryst. Growth **209**, 687 (2000).
[17] C.-H. Su, S. Zhu, N. Ramachandran, and A. Burger, J. Cryst. Growth **235**, 313 (2002).
[18] C.-H. Su, Thermochim. Acta **390**, 21 (2002).
[19] C.-H. Su, J. Cryst. Growth **281**, 577 (2005).
[20] C.-H. Su, W. Palosz, S. Zhu, S. L. Lehoczky, I. Grzegory, P. Perlin, and T. Suski, J. Cryst. Growth **235**, 111 (2002).
[21] R. F. Brebrick and A. J. Strauss, J. Phys. Chem. Solids **25**, 1441 (1964).
[22] Z. Remes, Ph.D. thesis, Charles University, 1999 (http://www.fzu.cz/~remes/thesis/thesis.html).
[23] S. Adachi, T. Kimura, and N. Suzuki, J. Appl. Phys. **74**, 3435 (1993).
[24] C.-H. Su, S. Feth, S. Zhu, S. L. Lehoczky, and L. J. Wang, J. Appl. Phys. **88**, 5148 (2000).
[25] M. Beaudoin, A. J. G. DeVries, S. R. Johnson, H. Laman, and T. Tiedje,

Appl. Phys. Lett. **70**, 3540 (1997).
[26]Y. P. Varshni, Physica (Amsterdam) **34**, 149 (1967).
[27]G. A. Slack and S. Galginaitis, Phys. Rev. **133**, A253 (1964).
[28]G. A. Slack, Phys. Rev. B **6**, 3791 (1972).
[29]J. A. Birch, J. Phys. C **8**, 2043 (1975).
[30]R. D. Greenough and S. B. Palmer, J. Phys. C **6**, 587 (1973).
[31]X. Mathew, J. Mater. Sci. Lett. **21**, 529 (2002).
[32]J. P. Laurenti, J. Camassel, A. Bouhemadou, B. Toulouse, R. Legros, and A. Lusson, J. Appl. Phys. **67**, 6454 (1990).
[33]S. Gilliland, J. Gonzalez, H. S. Guder, A. Segura, I. Mora, and V. Munoz, Phys. Status Solidi B **235**, 441 (2003).
[34]Y. Hwang, Y. Um, H. Kim, G. Jeen, and H. Park, J. Korean Phys. Soc. **34**, 405 (1999).
[35]T. S. Jeong and P. Y. Yu, J. Korean Phys. Soc. **43**, 1101 (2003).
[36]G. Fonthal, L. Tirado-Mejia, J. I. Marin-Hurtado, H. Ariza-Calderon, and J. G. Mendoza-Alvarez, J. Phys. Chem. Solids **61**, 579 (2000).
[37]L. S. Dang, G. Neu, and R. Romestain, Solid State Commun. **44**, 1187 (1982).
[38]W. Ehrenberg, Proc. Phys. Soc., London, Sect. A **63**, 75 (1950).
[39]E. O. Kane, J. Phys. Chem. Solids **1**, 249 (1957).
[40]J. L. Schmit, J. Appl. Phys. **41**, 2876 (1970).
[41]G. L. Hansen and J. L. Schmit, J. Appl. Phys. **54**, 1639 (1983).
[42]H. B. Bebb and C. R. Ratliff, J. Appl. Phys. **42**, 3189 (1971).
[43]J. D. Wiley and R. N. Dexter, Phys. Rev. **181**, 1181 (1969).
[44]M. Cardona and D. L. Greenaway, Phys. Rev. **131**, 98 (1963).
[45]F. T. J. Smith, Metall. Trans. **1**, 617 (1970).